



Efficient extraction of uranium (VI) from aqueous solution by Zr/Ce-UiO-66-NH₂ modified by dual strategies of bimetalization and amination

Wen-Hui Song¹ · Chen Wang¹ · Cheng-De Xie¹ · Zhi-Xiong Zhang¹ · Jian-Jun Wang¹

Received: 29 January 2024 / Revised: 14 March 2024 / Accepted: 25 March 2024 / Published online: 13 October 2024

© The Author(s), under exclusive licence to China Science Publishing & Media Ltd. (Science Press), Shanghai Institute of Applied Physics, the Chinese Academy of Sciences, Chinese Nuclear Society 2024

Abstract

We modified Zr/Ce-UiO-66-NH₂ using dual bimetalization and amination strategies to efficiently extract uranium from water resources. XRD, FTIR, and XPS indicated the successful alteration of material amination. Moreover, the metal Zr was partially replaced by Ce in Zr-oxygen atom clusters in Zr/Ce-UiO-66-NH₂. It possessed commendable structural stability in acidic and alkaline solutions. Irrespective of whether it was submerged in a 6 M strong acid or in a 0.5M strong base solution, the structural integrity of Zr/Ce-UiO-66-NH₂ remained unaffected. Batch experiments at pH = 6.0 revealed that uranium adsorption by Zr/Ce-UiO-66-NH₂ reached 376.8 mg g⁻¹ and 611.33 mg g⁻¹ at 298 K and 328 K, respectively. These values are much better than those obtained using bimetallic-modified Zr/Ce-UiO-66 or amine-functionalized UiO-66-NH₂. After five consecutive sorption and desorption cycles, the material retained a uranium removal rate of more than 80%, proving its excellent regenerative properties. Kinetic modeling of U(VI) adsorption on Zr/Ce-UiO-66-NH₂ implied that chemisorption dominated the rapid uranium sorption rate. We propose potential adsorption mechanisms involving three interactions: inner-sphere surface complexation, chemisorption, and electrostatic interactions. This study shows that the dual strategies of bimetalization and amination can effectively enhance U(VI) extraction from water. This approach has potential applications for the structural design of uranium adsorbents.

Keywords MOF modification · Zr/Ce-UiO-66-NH₂ · Adsorption uranium · Adsorption mechanism

1 Introduction

Fossil fuels, which are currently our primary energy source, have grown progressively scarcer, and the pollution caused by them and its impact on climate change are worrying [1]. Finding cleaner alternatives with large reserves has become necessary as fossil energy sources become insufficient to meet the escalating energy demand [2]. Nuclear energy is energy-dense, has a low environmental impact, and has

versatile applications. It can replace conventional energy sources in addressing the global energy crisis [3]. However, the negative impacts of energy applications are also emerging.

Uranium is the primary source of nuclear energy, and its mining and usage generate significant amounts of uranium-containing wastewater, which is highly toxic and radioactive. Owing to their high water solubility and very long half-life, UO₂²⁺ ions can spread throughout the environment via groundwater and surface water and potentially enter the human body. As a result, they pose a threat to both human health and ecosystems [4]. Like fossil fuels, nuclear power is a finite resource. Thus, uranium disposal and recycling are imperative from multiple standpoints [5].

Scientists have now devised various techniques for extracting hexavalent uranium, including ion exchange, chemical precipitation, membrane dialysis, bioconcentration, solid-liquid separation, and adsorption [6]. Although these approaches have been used to treat radioactive effluents [6,

This work was supported by the National Natural Science Foundation of China (No. 22376058).

✉ Jian-Jun Wang
wangjj2016@ncepu.edu.cn

¹ MOE Key Laboratory of Resources and Environmental Systems Optimization, College of Environmental Science and Engineering, North China Electric Power University, Beijing 102206, China

7], they have limitations regarding treatment effectiveness and production applications, including suboptimal treatment outcomes, high costs, and regeneration difficulties [6, 7]. In contrast, adsorption is widely acknowledged for its extensive applications owing to its uncomplicated operation, cost-effectiveness, eco-friendliness, and superior selectivity for uranium [6, 8, and 9].

The effectiveness of adsorbent materials is defined as their pollutant removal efficiency in adsorption. Previously reported adsorbent materials, like biopolymers, clays, and nanomaterials, are not ideal uranium adsorbents because of their limitations, such as high processing costs, limited adsorption properties, poor chemical and water stability, and poor reusability [7, 9]. Hence, materials with better uranium removal properties are required to overcome these limitations.

Metal-organic frameworks (MOFs) are highly organized and porous structures with exceptional characteristics, such as large active specific surface areas, enriched reactive sites, and manifold structural variety [10]. Because of their distinct properties, MOFs have the potential to overcome the problems associated with traditional adsorbents and exhibit high U(VI) adsorption capabilities. As a result, MOFs have been successfully used to remove uranium from aquatic environments [11].

UiO-66 is a rigid metal-organic framework material comprising metal-oxygen clusters ($Zr_6O_4(OH)_4$) and terephthalic acid (H_2BDC) [12]. Since its initial discovery by Cavka et al. [13], UiO-66 has sparked significant research interest in numerous research groups around the globe. The solvothermal and chemical stabilities of UiO-66-Zr are the direct result of its unique pore architecture and high coordination number [14]. Nevertheless, its effectiveness as a uranium adsorbent is restricted due to its poor adsorption properties [15, 16].

Nitrogen atoms are soft ligands with a strong affinity for light actinides [17, 18]. One study revealed that the amino group can promote electrostatic interactions between MOFs and substrates, while providing an active site for adsorption [19]. Therefore, incorporating functional amines into porous MOFs can significantly enhance uranium extraction performance. For instance, in contrast to UiO-66, UiO-66-NH₂ exhibits excellent U(VI) sorption. Additionally, it exhibits exceptional hydrostability and adsorption performance [20].

Ce(III) is an inexpensive and nontoxic rare-earth metal belonging to the same group as Zr. It is characterized by stability and rapid changes in its valence state [21]. It has applications in various disciplines, including optics, catalysis, and electricity [22]. Its exceptional stability ensures that its properties remain unchanged even after the addition of other functional groups [23, 24]. Previous studies [25] have demonstrated that Ce-based UiO-66 exhibits excellent

physicochemical stability and that the presence of cerium ions promotes material-substrate interactions [26]. In particular, Ce(IV) has strong Lewis-acid properties that enhance the adsorption of uranium by the material. The 4f orbital of Ce(IV) can also interact with the P=O bond to facilitate the reaction [27]. Wang et al. [28, 29] presented the initial evidence that incorporating Ce(III) into UiO-67 alters the surface charge, nature, content of sorption spaces and sites, and electrostatic and π - π interactions, all of which affect the sorption properties of the material.

In this study, a simple method was employed to synthesize octahedral structured nanomaterials of Zr/Ce-UiO-66-NH₂ modified by the dual strategies of bimetalization and amination. Various characterization methods have been applied to observe the microstructure of substances. Batch experiments were conducted to determine the U(VI) adsorption performances of the materials and explore their applicability. The behavior of material adsorption and the potential adsorption mechanisms are described. This dual-modified material has a significant potential for application in the treatment of uranium-bearing wastewater.

2 Results and discussion

2.1 Characterization

We performed XRD on the synthesized materials, as shown in Fig. 1a, and all samples exhibited satisfactory crystallinity. Zr/Ce-UiO-66-NH₂ showed characteristic peaks at 7.6° (111), 8.6° (220), and 25.8° (442). Experiments have demonstrated that the structure of the research materials remains unchanged when doped with Ce. In other words, introducing other metals may not destroy the structure of MOFs. The images show that the material exhibits superior crystal structure and crystallinity. Notably, Zr/Ce-UiO-66 displays similar diffraction peaks, indicating that the inclusion of amino groups did not affect the material structure [30–32]. There was a decrease in the peak intensity at 8.6° in materials with bimetallic central sites, as opposed to UiO-66-NH₂, which has significant monometallic sites. This phenomenon may be due to the partial substitution of Ce by Zr, which caused the formation of a cerium-oxygen structure, resulting in a reduction in the number of zirconium-oxygen clusters. This indicates that the Ce doping affected the crystallinity of the samples [33].

As shown in Fig. 1b, the FT-IR image was comparable to that of UiO-66-NH₂, which indicates that the inclusion of Ce(III) does not disrupt the metal-organic material skeleton. This agrees with existing evidence [33]. The image shows distinct absorption peaks at approximately 1585 cm⁻¹, 1431 cm⁻¹, and 1396 cm⁻¹. These peaks may be due to the asymmetric and symmetric stretching

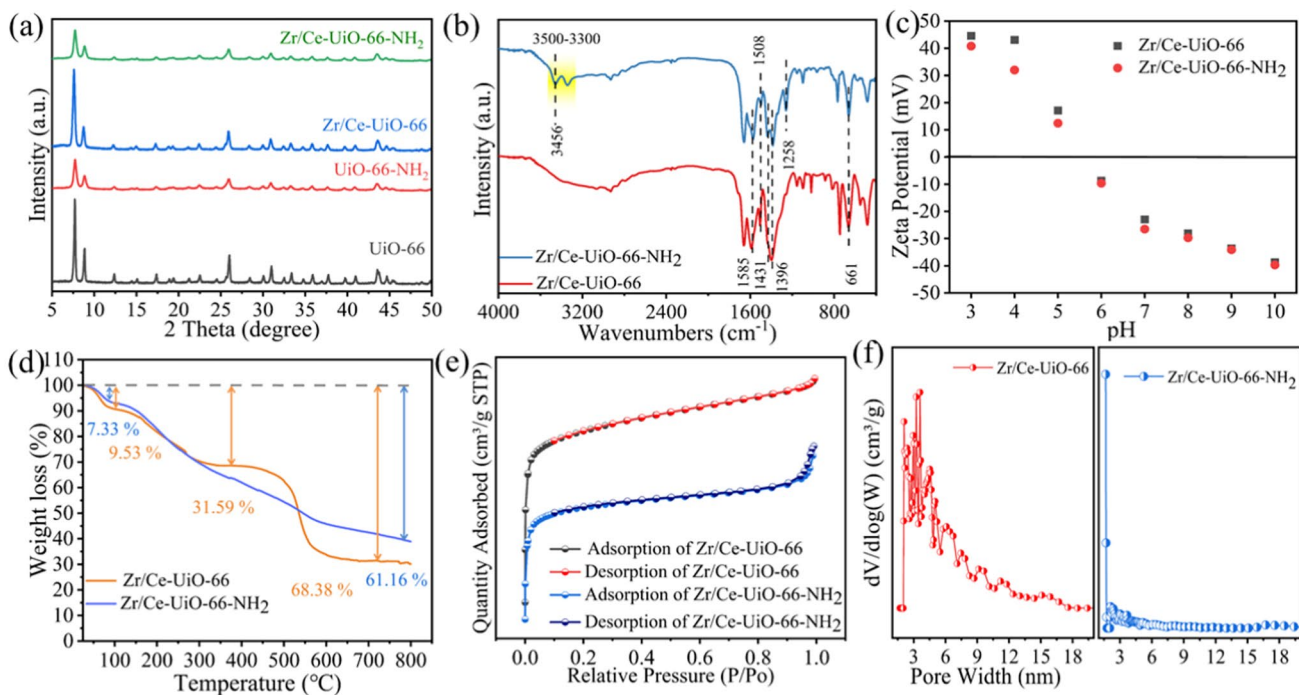


Fig. 1 Characterization of Zr/Ce-UiO-66 and its derivatives: **a** XRD; **b** FT-IR; **c** Zeta potential; **d** thermogravimetric curve; **e** nitrogen adsorption–desorption isotherms; **f** pore size distributions. (Color figure online)

vibrations of the carboxyl groups in the ligands of the synthesized materials [34]. In addition, the absorption peaks at 1450–1580 cm^{-1} are strongly connected to the C=C vibrations of the H₂BDC ligands [35]. For both materials, a spectral range of 600–800 cm^{-1} was observed, which coincides with the spectral range of Ce–O and Zr–O bonds. In particular, researchers have identified the asymmetric stretching vibrations of O–Zr–O near 661 cm^{-1} [34, 35]. Previous reports have indicated that the interaction between elemental Ce and the ligand leads to the formation of Ce–O and Ce–C bonds. The absorption peak at 1502 cm^{-1} in Fig. 1b reinforces this viewpoint. The presence of this peak verifies the successful doping of Ce metal in the MOFs [36]. The spectrum of Zr/Ce-UiO-66-NH₂ exhibited moderate double peaks within the 3500–3300 cm^{-1} range. The 3453 cm^{-1} and 1258 cm^{-1} peaks align with the stretching vibrations of N–H and C–N, respectively. The results of these experimental tests confirmed the successful integration of -NH₂ into the Zr/Ce-UiO-66 structure [37].

The SEM plots shown in Fig. 2a and Fig. S1(a, b, c) illustrate that the regular structures of both modified MOF materials remained intact. The structure of Zr/Ce-UiO-66-NH₂ was ortho-octahedral in shape, similar to the typical structures of UiO-66-NH₂ containing single-metal sites. The introduction of Ce metal led to the adhesion and binding of nanoparticles, whereas the MOF particles exhibited strong

aggregation. TEM was used to analyze the morphologies of the modified MOFs. Figures 2b, S1d, and 2(b, c) show the typical octahedral structures of Zr/Ce-UiO-66 and Zr/Ce-UiO-66-NH₂, corresponding to their SEM images. By comparing Fig. 2(b,c), it is clear that introducing amino groups increases the dip-sticking ability of the material and causes it to agglomerate. However, owing to the low crystallinities of the materials, these images did not show distinct lattice streaks [38].

The EDS patterns shown in Fig. 2d and Fig. S1e indicate Ce(III) doping. The composites found in the MOFs consist of C, N, O, Zr, and Ce, and their presence in the test area agrees with the morphology of the materials. The SEM, TEM, and EDS results indicated that the solvothermal technique effectively produced bimetallic MOFs.

The elemental species and valence states of the prepared samples were analyzed using XPS. The complete spectrum scan (Fig. 3e) shows clear peaks corresponding to the five elements, which agrees with the elemental species identified by EDS (Figs. 2e and S1e). This observation further confirms that the bimetallic material Zr/Ce-UiO-66 and dual-strategy-modified Zr/Ce-UiO-66-NH₂ were successfully synthesized. Figures 3a and Ref. 4 show high-resolution XPS C 1s spectra. Figure 4a shows three distinct peaks at 284.80 eV, 286.10 eV, and 288.80 eV corresponding, respectively, to the binding energies of the C–C, C=C, and O–C=O bonds reported in the literature [39]. These characteristic

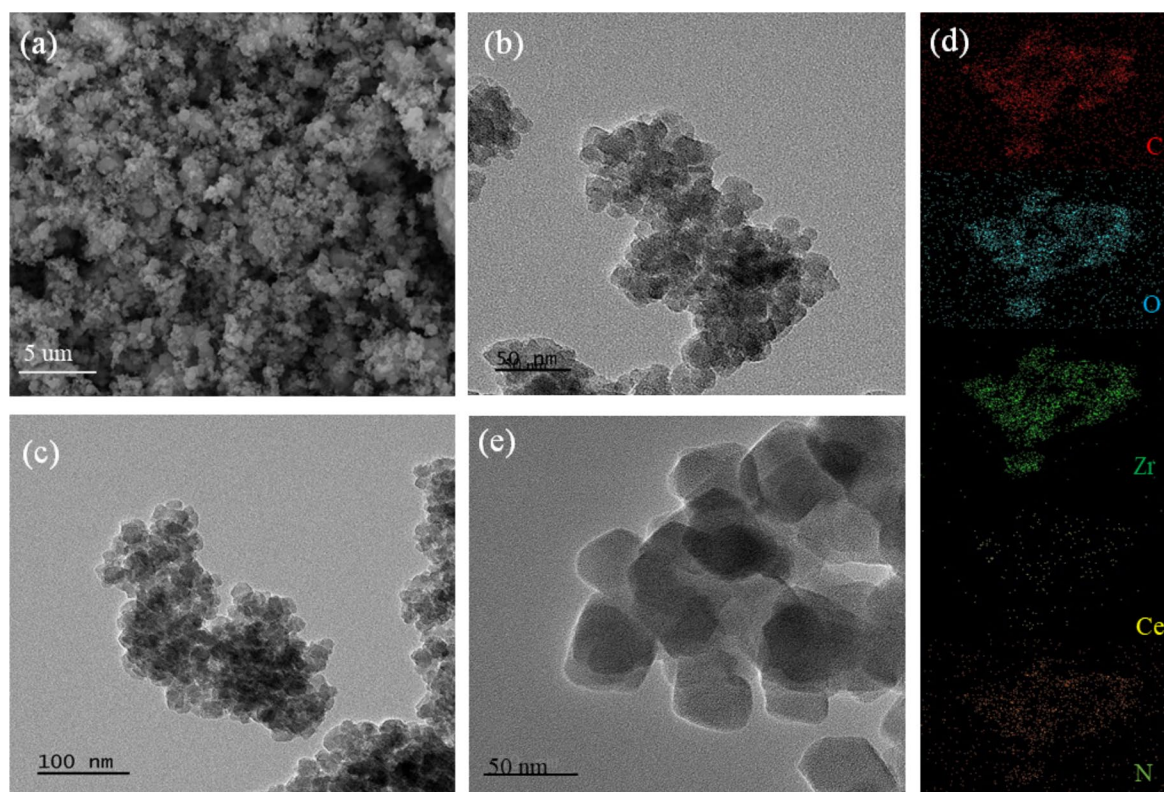


Fig. 2 Zr/Ce-UiO-66-NH₂: **a** SEM; **b, c** TEM; **d** EDS. Zr/Ce-UiO-66; **e** TEM. (Color figure online)

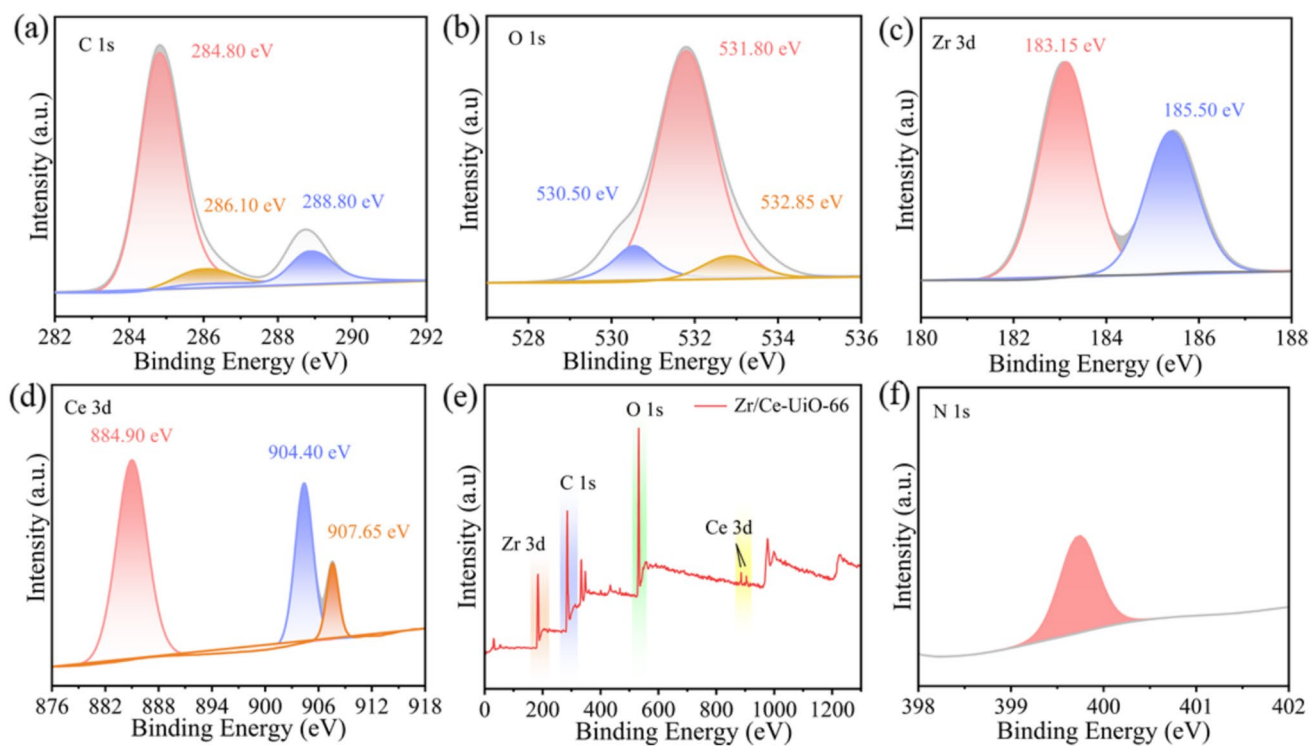


Fig. 3 XPS spectra of Zr/Ce-UiO-66: **a** C 1s, **b** O 1s, **c** Zr 3d, **d** Ce 3d, **e** full spectrum. **f** N 1s spectrum of Zr/Ce-UiO-66-NH₂-U. (Color figure online)

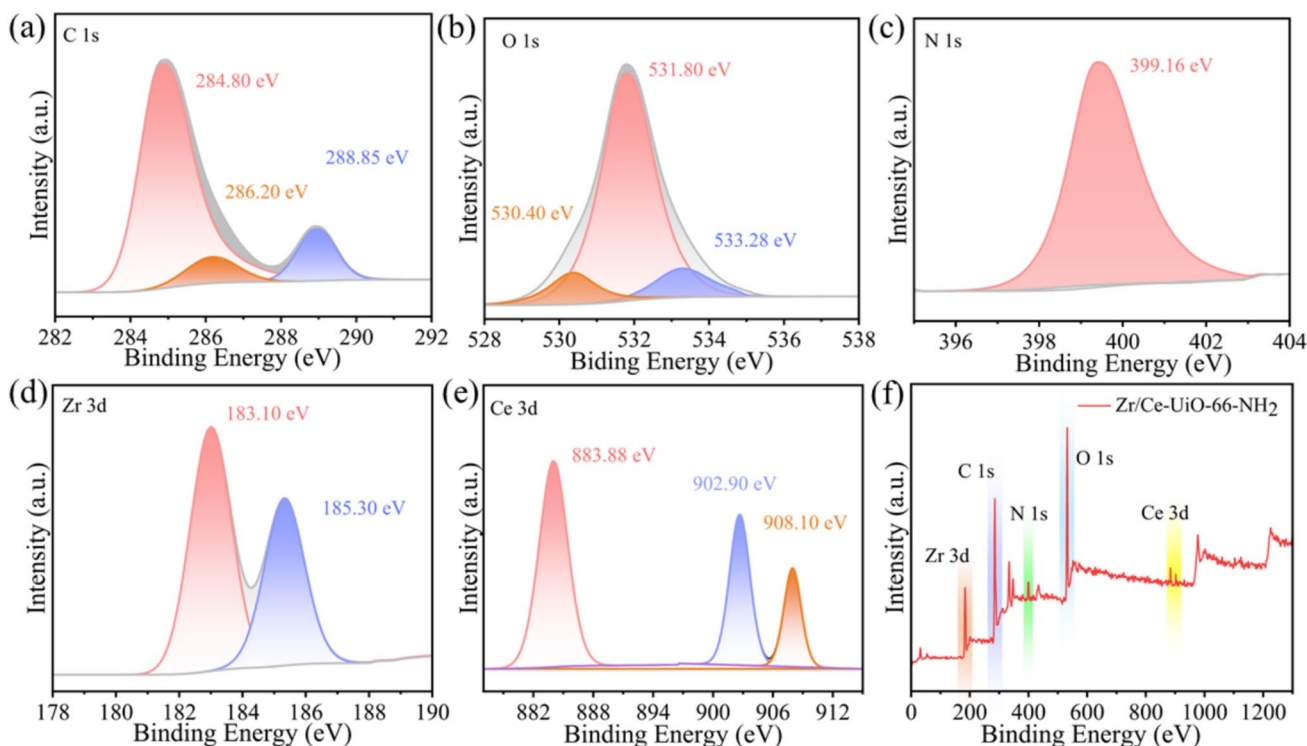


Fig. 4 XPS spectra of Zr/Ce-UiO-66-NH₂: **a** C 1s, **b** O 1s, **c** N 1s, **d** Zr 3d, **e** Ce 3d, **f** full spectrum. (Color figure online)

peaks are similar to those observed for UiO-66 [40], which occur at 183.15 eV and 185.50 eV, as shown in Fig. 3c, and at 183.10 eV and 185.50 eV, as shown in Fig. 4d, corresponding to the Zr 3d_{5/2} and Zr 3d_{3/2} binding energies [40]. The characteristic N 1s spectrum at 399.16 eV is consistent with the manifestation of the amino peak in MOFs [41, 42] and agrees with the FTIR spectral characterization. In both materials, as shown in Fig. 3b, the O 1s spectra reveal characteristic peaks at 532.85 eV, 531.80 eV, and 530.50 eV. In Fig. 4b, they can be observed at 533.28 eV, 531.80 eV, and 530.40 eV. As previously discussed, the oxygen-related peaks described above are generated by the C–O, C=O, and Zr–O bonds [8]. A characteristic peak, similar to that of UiO-66, was identified to be that of Ce metal, which can replace Zr, leading to the presence of Ce–O with a peak location equivalent to that of Zr–O [43].

In addition, the peaks at 884.90 eV and 904.40 eV in Fig. 3d and at 883.38 eV and 902.90 eV in Fig. 4e indicate the presence of Ce³⁺ in both materials. In contrast, the 907.65 eV and 908.10 eV peaks were identified as Ce⁴⁺ [36]. However, the elemental peak at 917 eV is absent in Fig. 4e, indicating the absence of or existence of a very small amount of Ce⁴⁺ in this material. This implies that while Ce is abundant, it mainly exists as Ce³⁺ [35].

TGA analyzes the thermostability of materials in the range of 20–800 °C. During the initial thermal treatment

stage, Zr/Ce-UiO-66 and Zr/Ce-UiO-66-NH₂ underwent mass losses of approximately 9.53% and 7.33%, respectively, which occurred mainly because of the thermal volatilization of the water polymer in the pore channels up to 200 °C. The subsequent process involved slower pyrolysis of the materials. The mass loss in the temperature range of 200–800 °C is primarily explained by the collapse and degradation of the organic skeleton of the MOF. Notably, approximately 31.62% and 38.84% of the mass remained, implying that the material was thermally stable (Fig. 1d).

Porosity is an important quality indicator for synthesized materials. N₂ adsorption–desorption experiments conducted at 77 K were used to investigate the BET area and apertures of the material. Figure 1d shows the calculated surface areas of 974.67 m² · g⁻¹ and 642.06 m² · g⁻¹, indicating substantial specific surface areas. Figure 1d shows a microporous structure with a pore size similar to that of Zr/Ce-UiO-66 concentrated at 3.28 nm, while the pore size is 1.67 nm for Zr/Ce-UiO-66-NH₂. From the data in Fig. 1d and f, it is evident that the modification strategy of amino functionalization resulted in a decreasing trend for both indicators. Zr/Ce-UiO-66-NH₂ exhibits a relatively high specific surface area, which enables excellent U(VI) adsorption owing to the increased number of active sites.

2.2 Adsorption experiments

2.2.1 Effect of pH

The pH of the reaction system significantly affects the distribution of uranium in water and the surface nature of the material [28]. Uranium solutions with a concentration of $10 \text{ mg} \cdot \text{L}^{-1}$ were allowed to adsorb onto Zr/Ce-UiO-66-NH₂ at pH 2–10 for 6 h. Figure 5a shows that the adsorption capacity of both adsorbents was low at pH levels of 2–4, increased rapidly at pH levels of 5–8, peaking at a pH of 8. Subsequently, a declining trend was observed for pH values of 8–10. The Zr/Ce-UiO-66 material with bimetallic central sites demonstrated a significantly superior U(VI) removal effect compared to UiO-66 with single metallic sites. Additionally, Zr/Ce-UiO-66-NH₂, which was modified using a dual strategy, exhibited a higher U(VI) removal effect than the bimetallic-modified Zr/Ce-UiO-66 and purely amino-chemical-modified UiO-66-NH₂. These results indicate the promising potential of the newly synthesized materials for practical applications. The superior adsorption capacity of bimetallic materials compared to that of monometallic materials may be attributed to the high Lewis-acid properties of Ce. Furthermore, the 4f orbital of Ce(IV) interacts with the P=O bond to facilitate the reaction [26]. At the same time,

the presence of cerium ions promotes material-substrate interactions [25]. The performance of Zr/Ce-UiO-66-NH₂ was superior to Zr/Ce-UiO-66, which may be attributed to the introduction of an amino group, which led to an increase in the number of binding sites.

Uranium exists in various ionic forms at different pH values. Figure S2 shows the proportional occurrence of various forms of uranium in aqueous solutions at different pH levels. In acidic environments, UO_2^{2+} is typically the dominant positively charged species [43]. As the pH increases, chemical precipitation occurs in the uranyl solutions. Figure 1c shows that, at pH 6, the surface of the material carries a negative charge. At this pH, uranium existed in its positively charged hexavalent form. The resulting electrostatic attraction enhanced the U(VI) adsorption ability. At high pH (pH > 8), the primary U(VI) species are $\text{UO}_2(\text{CO}_3)_3^{4-}$ or $\text{UO}_2(\text{OH})_3^{3-}$, which are insoluble in water [43, 44]. Under these conditions, uranium was eliminated via material adsorption and physical precipitation. The zeta data shown in Fig. 1c further substantiate the previously inferred sorption behavior. At a lower pH of 2–5, the zeta data for both materials were positive, indicating a favorable charge on the surface of both adsorbents. Under these circumstances, uranium predominantly exists as a positively charged UO_2^{2+} . Electrostatic repulsion leads to a significantly lower adsorption capacity.

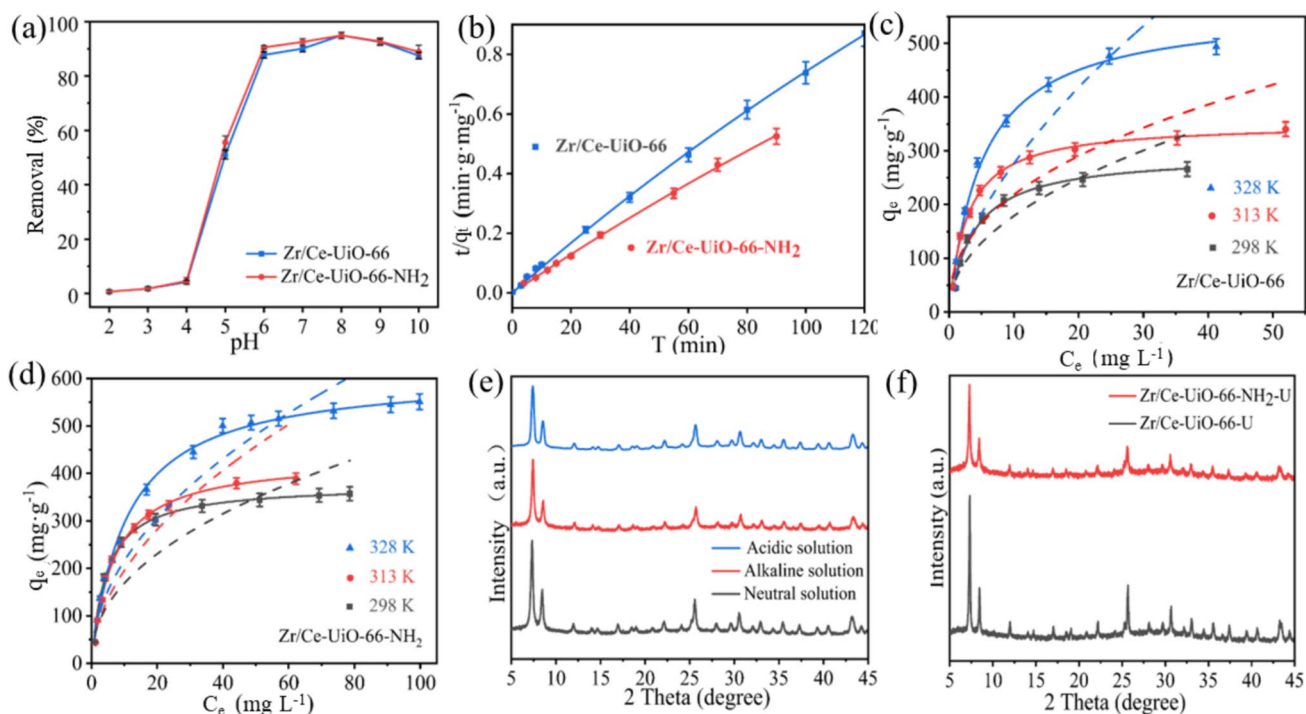


Fig. 5 Zr/Ce-UiO-66 and Zr/Ce-UiO-66-NH₂: **a** Impact of varying pH levels during U(VI) sorption at 298 K; **b** pseudo-second-order curves of the adsorption of U(VI) onto various adsorbents at $m/V = 0.1 \text{ g/L}$, C_0 (U(VI)) = $50 \text{ mg} \cdot \text{L}^{-1}$; **c**, **d** sorption isotherms of U(VI) at $T = 298 \text{ K}$, 313 K , 328 K ; the solid lines represent the Langmuir

model and the dashed lines represent the Freundlich model. **e** XRD pattern of Zr/Ce-UiO-66-NH₂ after acid–base neutral solution immersion; **f** XRD pattern of Zr/Ce-UiO-66-U and Zr/Ce-UiO-66-NH₂-U. (Color figure online)

Nevertheless, at pH 6, the surfaces of both materials possessed a negative charge, and hexavalent uranium existed primarily as a polymer of UO_2^{2+} . This generated more electrostatic attraction, thereby leading to enhanced adsorption capacity.

Although both materials performed more efficiently in eliminating uranium under alkaline conditions, higher pH levels in the range of the studied uranium concentrations caused precipitation [43]. This implies that the experimental results only partially reflect the adsorption characteristics. This study focused on the treatment of weakly acidic nuclear wastewater. Moreover, the two substances displayed satisfactory adsorption capabilities at pH 6. Therefore, considering all these factors, the adsorption experiments were conducted at pH 6.

2.2.2 Ionic strength effects

Ionic strength dependence is a valuable tool for identifying complexes on inner and outer surfaces. In the less dependent scenario, inner surface complexes are believed to be formed through adsorption [44]. This study examined the effects of U(VI) adsorbability on Zr/Ce-UiO-66 and Zr/Ce-UiO-66-NH₂ at different concentrations of NaNO₃. In the adsorption experiment, various amounts of NaNO₃ were added to an aqueous solution containing 10 ppm of uranium, and the solution was incubated for 6 h. A close examination

of Fig. 6e and f shows that the alterations in the adsorption curves are nearly imperceptible, even with a change in NaNO₃ concentration. This indicates that ionic strength does not interfere with the sorption process of uranium ions. In other words, changes in ionic strength did not significantly interfere with the sorption behavior of the uranium ions. This observation confirmed our hypothesis that uranium ions were adsorbed onto the material by chemically binding to the active sites on its surface and creating internal surface complexes.

2.2.3 Effect of coexisting ions

Wastewater discharged from the nuclear industry contains numerous ions, in addition to U(VI). The presence of these ions may significantly interfere with U(VI) removal efficiency. Hence, it is imperative to investigate the impact of different electrolyte ions (including the anions NO_3^- , Cl^- , CO_3^{2-} , SO_4^{2-} , and K^+ , Co^{2+} , Ni^{2+} , mg^{2+} , Sr^{2+} , Zn^{2+} , and Ca^{2+}) on uranium elimination. The removal effects of the adsorbent are shown in Figs. 6a and 6b. The efficiencies of Zr/Ce-UiO-66 and Zr/Ce-UiO-66-NH₂ for the removal of hexavalent uranium in the presence of Ca^{2+} were 62.4% and 69.6%, respectively, and in the presence of Sr^{2+} , they were 69.6% and 63.6%, respectively. The formation of a ternary Ca^{2+} -uranyl complex affects the migration of hexavalent uranium in water. Such a construction may result in a lower solubility

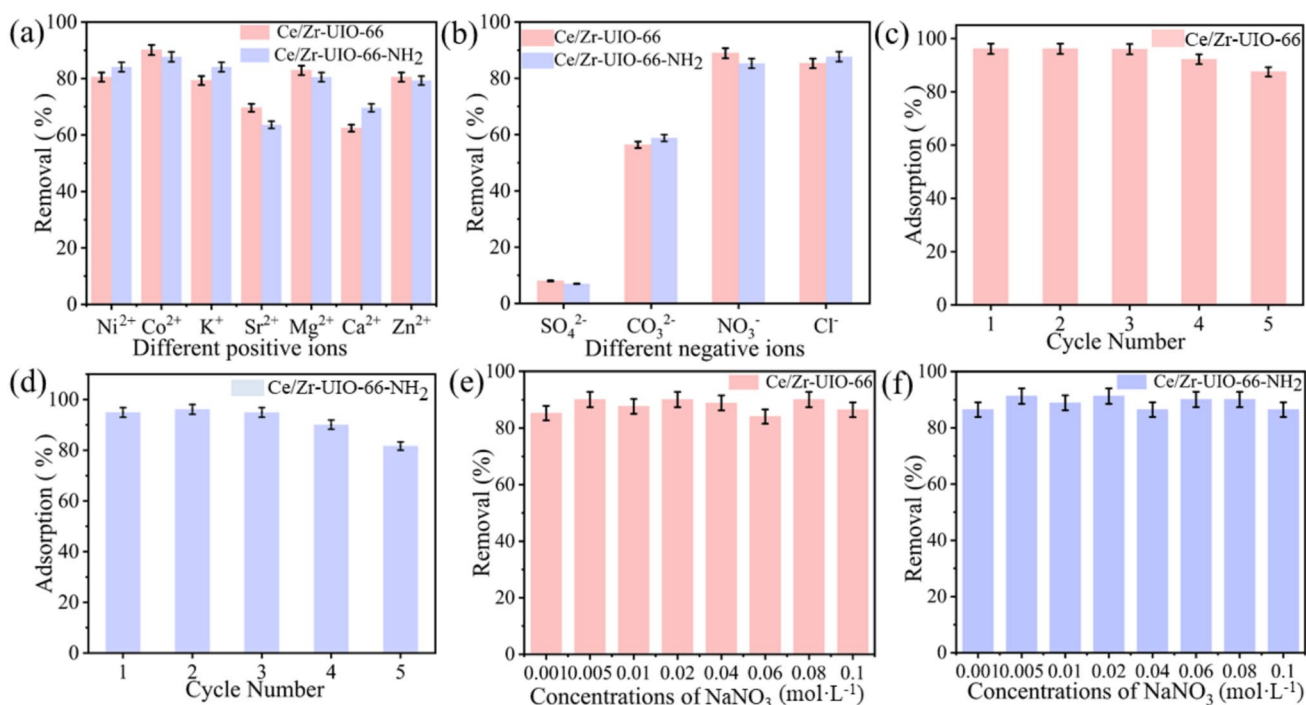


Fig. 6 Zr/Ce-UiO-66 and Zr/Ce-UiO-66-NH₂ at pH = 6 and $T = 298$ K: **a** cations and **b** anions cations during U(VI) sorption at $C_0 = 10$ $\text{mg} \cdot \text{L}^{-1}$, $m/V = 0.1$ g/L ; **c**, **d** sorption recyclability after five

cycles; **e**, **f** effect of different concentrations of NaNO₃ during U(VI) sorption. (Color figure online)

and mobility of hexavalent uranium [45]. The presence of Sr(II) in the aqueous solution partially overlapped with the U(VI) adsorption sites, which included oxygen-containing functional groups ($-\text{OH}$, $-\text{C}-\text{O}-\text{C}$, and $-\text{COOH}$). This overlap results in competition for adsorption between the two ions, which affects the U(VI) adsorption by the material [49]. The CO_3^{2-} and SO_4^{2-} anions significantly affected the adsorption performance of the materials, resulting in removal efficiencies of only 56.3% and 3.37%, respectively, for hexavalent uranium in Zr/Ce-UiO-66, and 58.8% and 2.17%, respectively, in Zr/Ce-UiO-66-NH₂. SO_4^{2-} forms new, highly stable complexes with uranyl ions that significantly diminish the adsorption properties of the material [28]. Carbonates readily form negatively charged U(VI)-carbonate complexes, which do not get adsorbed easily on most materials [50]. Although the magnitudes of ion effects on the two materials varied, overall, they were comparable. The effect of these ions on Zr/Ce-UiO-66-NH₂ in terms of U(VI) adsorption was slightly smaller than on Zr/Ce-UiO-66. This difference can be attributed to the introduction of an amino group, which increases the number of binding sites.

In this study, the adsorption of various ions onto U(VI) was experimentally measured. The histograms in Fig. 6a and b show that ions other than the four ions mentioned previously have minimal influence on the adsorption of U(VI). Therefore, when considering the effects of Zr/Ce-UiO-66-NH₂ on the adsorption of U(VI), the focus should be on internal surface complexation.

2.2.4 Adsorption kinetics

The practical applicability of MOFs is derived from their adsorption kinetics. The rates of adsorption of U(VI) onto Zr/Ce-UiO-66-NH₂ were examined by maintaining the substrate concentration at $50 \text{ mg} \cdot \text{L}^{-1}$ and measuring the U(VI) concentrations at different time intervals. Figure 5b shows that the adsorption kinetics of Zr/Ce-UiO-66 were relatively slow, requiring almost two hours to reach equilibrium. Meanwhile, the adsorption of U(VI) onto Zr/Ce-UiO-66-NH₂ occurred quickly in the first forty min, followed by gradual equalization, requiring approximately one hour to reach equilibrium. This increased adsorption rate of Zr/Ce-UiO-66-NH₂ may have been caused by the presence of actinide soft-donor amino groups, increased affinity for uranium ions, and multiple uptake sites [18]. Initially, the material offers abundant uranium-binding sites to absorb considerable quantities of U(VI). Upon contact with U(VI), the adsorptive ability increases dramatically owing to transient sorption or adsorption on the outer surface. As the adsorption progresses, most of the surface sites are occupied. The resulting U(VI) diffuses inward and adheres to the active sites within the substance for further adsorption. This results

in a broader U(VI) diffusion range and decreased adsorption rate [46].

As shown in Table 1, to obtain insights into the dynamics of U(VI) adsorption on the two materials, we applied two kinetic models, namely the pseudo-first-order and pseudo-second-order kinetic models, to the observed test data (Eqs. (5) and (6) in the Supporting Information). Figure 5b shows that Zr/Ce-UiO-66-NH₂ reaches kinetic equilibrium within 50 min. Under the same conditions, the dual-strategy-modified Zr/Ce-UiO-66-NH₂ reached adsorption equilibrium significantly earlier than the single-strategy-modified Zr/Ce-UiO-66. The adsorption of U(VI) onto Zr/Ce-UiO-66-NH₂ is described well by the proposed second-order kinetics, as demonstrated by an R^2 value of 0.999 and q_e value of 216.16 mg g^{-1} . This indicates that the chemisorption mechanism primarily controls the uranyl adsorption rate of this material [47].

2.2.5 Adsorption isotherms

Temperature is one of the most significant factors that influence chemisorption. We studied uranium sorption on Zr/Ce-UiO-66-NH₂ and determined the type of adsorption reaction. Batch experiments were conducted on uranium by using a substrate concentration gradient of $10\text{--}200 \text{ mg} \cdot \text{L}^{-1}$. The experiment was performed at temperatures of 298 K, 313 K, and 328 K and a pH of 6. The maximum sorption ability of the synthesized adsorbent was determined by studying the adsorption isotherms. It was found that with increasing uranium concentration, the adsorption capacity increased for the entire concentration range studied. The previously reported optimal sorption capacity of UiO-66-NH₂ was approximately 114.4 mg g^{-1} under equivalent pH conditions [19]. Meanwhile, we synthesized Zr_x/Ce-UiO-66-NH₂ ($x = 2, 1, 0.5$) with different Zr:Ce ratios (2:1, 1:1, 1:2) and conducted adsorption experiments at pH 6 and 298 K. The XRD plots in Fig. S4 show that the three materials were well crystallized. The results, as shown in Fig. S5, indicate that the adsorption performance of Zr/Ce-UiO-66-NH₂ was better when the Zr:Ce ratio was 1:1. Figure 5c and d illustrate the adsorption effects of Zr/Ce-UiO-66-NH₂ at 298 K, 313 K, and 328 K and pH 6. The results indicated that at pH = 6.0 and 298 K, the adsorptive ability of Zr/Ce-UiO-66-NH₂, which was modified by the dual strategy, was 376.8 mg g^{-1} . The adsorption capacity of Zr/Ce-UiO-66, which was modified only by bimetallic modification, was 293.8 mg g^{-1} , and that of UiO-66-NH₂, which was modified only by amination, was 114.4 mg g^{-1} [19]. The above data reveal that the dual-strategy-modified materials performed significantly better. At 313 K and 328 K, the material exhibited a U(VI) extraction capacity of 433.84 mg g^{-1} and 611.33 mg g^{-1} , respectively. The data show the maximum amount of adsorbent at various temperatures. Both isotherms

exhibit an ascending gradient with increasing temperature, indicating that high temperatures promote adsorption. As shown by these experiments, Zr/Ce-UiO-66-NH₂, which was modified through bimetallic and amination methods, demonstrated a superior ability to adsorb U(VI).

The experimental data were fitted to two well-established models, the Langmuir and Freundlich models, to determine the agreement of the experimental data with the digital data and explain the adsorptive process. The data in Table 2 align more closely with the Langmuir model, as shown by the R^2 values. As shown above, the results illustrate that the active sorption sites were uniformly distributed across the adsorbent, forming a monolayer on the surface of the adsorbent. The results indicate that Zr/Ce-UiO-66 and Zr/Ce-UiO-66-NH₂ adsorbed 293.8 mg g⁻¹ and 376.8 mg g⁻¹ of U(VI), respectively, at 298 K, which is consistent with the recorded data. Moreover, the adsorption performances of both nanomaterials were superior to those of many other MOFs. Incorporating Ce enhances the interactions between the material [28] and U(VI), and integrating amino groups increases the number of available binding sites [18]. Both the materials in this study exhibited exceptional adsorption properties, which makes them ideal adsorbents for the eradication of radionuclides (Table 3).

2.2.6 Recyclability

To evaluate the application potential of an absorbent, its reusability must be considered. Each material was dissolved at 10 mg in 100 mL of uranium solution at 10 ppm and pH 6.0. The reaction was allowed to progress for 12 h on a shaker. A centrifuge was used for solid–liquid separation, and the supernatant was tested for uranium content. The solid phase was submerged in a solution of 0.5 M Na₂CO₃ for 6 h to facilitate desorption. The soaked material was washed with ultrapure water until it reached neutrality, and then dried under vacuum to yield the resulting material for the subsequent cycle. This process was repeated five times, and the uranium removal efficiency was determined for each trial. Figure 6c and d show that more than 80% of the initial amount of uranium was recovered from Zr/Ce-UiO-66 and Zr/Ce-UiO-66-NH₂ after five cycles. These results indicate that the sorption efficiencies of both materials remained unaffected. Both materials exhibit excellent recyclability and can thus be used continuously for wastewater treatment over long periods.

Next, both MOFs were submerged in acidic, alkaline, and neutral solutions with varying pH values for 24 h. Subsequently, the material was washed to a neutral pH, and the resulting precipitate was dried by centrifugation and analyzed using XRD. As shown in Fig. 5e and f, the structural integrity of the MOFs remained unaffected after submersion in a 6 M HCl or 0.5 M NaOH aqueous solution. These

findings show that the MOFs possess high structural stability in acidic and alkaline solutions, an exceptional capacity for resisting acids and chemicals, and the potential for effective practical applications.

3 Possible adsorption mechanism

Chemisorption and physisorption are widely accepted methods for separating heavy metal ions from powdered materials. We conducted numerous experiments to ascertain potential adsorption mechanisms of U(VI) on Zr/Ce-UiO-66 and Zr/Ce-UiO-66-NH₂, including FTIR, XRD, zeta potential, and XPS. Under different pH conditions, Zr/Ce-UiO-66-NH₂, which contained bimetallic central sites, exhibited superior uranium removal performance compared to Zr/Ce-UiO-66 or UiO-66-NH₂. Notably, the uranium sorption properties of Zr/Ce-UiO-66-NH₂, which was modified by the dual strategy of bimetallicization and amination, were further improved compared to those of Zr/Ce-UiO-66. This indicates that the newly produced substance has better potential for application. The increase in the ability of Zr/Ce-UiO-66-NH₂ to absorb uranium might have resulted from the addition of Ce to UiO-66 during the synthesis, which may lead to isomorphous substitutions that generate faults, thus revealing more acidic locations. The enhanced uranium adsorption properties of this material may be attributed to several factors, including Ce(IV), which has strong Lewis-acid properties, and the 4f orbital of Ce(IV). Furthermore, Ce enhances the interactions between the substance and U(VI) [25, 26]. The high uranium sorption performance of Zr/Ce-UiO-66-NH₂ could also be linked to the presence of an amino group, which increases the number of available binding sites [18]. Zeta potential testing indicated that Zr/Ce-UiO-66-NH₂ was negatively charged at pH 6, suggesting a higher electrostatic interaction between the surface adsorbent and the UO₂²⁺ ion (Fig. 1c).

Using XRD, the changes in Zr/Ce-Ui-O-66 and Zr/Ce-Ui-O-66-NH₂ before and after uranium adsorption were determined to investigate the chemical stability of the two materials, as shown in Fig. 5f. The XRD patterns of the native and uranium-loaded samples showed no noticeable discrepancies. This indicates that the crystal structure of Zr/Ce-UiO-66-NH₂ remained unchanged after U(VI) adsorption. The changes in Zr/Ce-UiO-66-NH₂ after uranium adsorption were scrutinized using XPS, as shown in Figs. 7 and 8. The spectra of the two substances and high-fraction XPS spectrum of U 4f were compared. The analysis indicates that the peaks of U 4f_{5/2} and U 4f_{7/2} correspond, respectively, to the peaks at 392.80 eV and 382.10 eV in Fig. 7e and 392.55 eV and 382.70 eV in Fig. 8e. The results confirmed that the material reliably adsorbed uranium. The UiO-66 framework cell contained two variants of Zr–O bonds. One was the

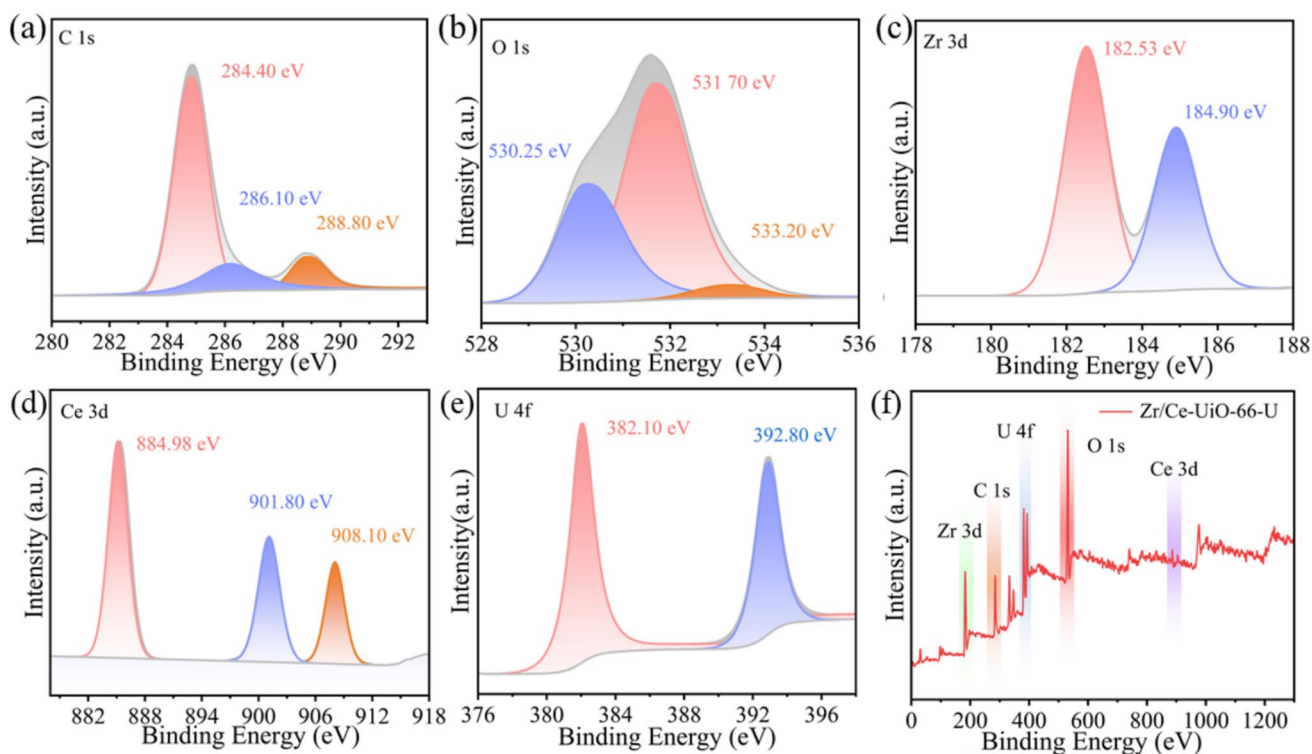


Fig. 7 High-resolution XPS spectra of Zr/Ce-UiO-66-U: **a** C 1s, **b** O 1s, **c** Zr 3d, **d** Ce 3d, **e** U 4f, and **f** full spectrum. (Color figure online)

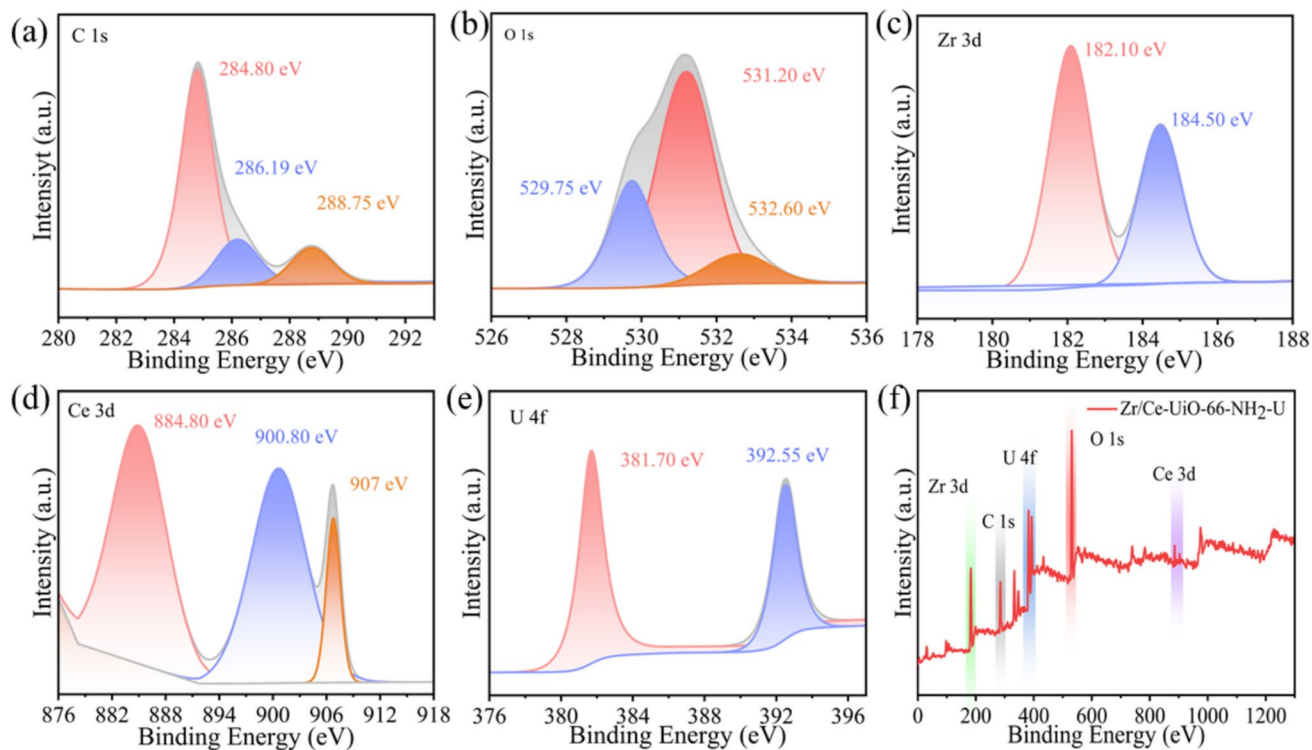


Fig. 8 High-resolution XPS spectra of Zr/Ce-UiO-66-NH₂-U: **a** C 1s, **b** O 1s, **c** Zr 3d, **d** Ce 3d, **e** U 4f, and **f** full spectrum. (Color figure online)

Table 1 Kinetic model fitting results for U(VI) adsorption on Zr/Ce-UiO-66 and Zr/Ce-UiO-66-NH₂

Adsorbent	Pseudo-first-order			Pseudo-second-order		
	K_1	q_e (mg g ⁻¹)	R^2	K_2	q_e (mg g ⁻¹)	R^2
Zr/Ce-UiO-66	0.243	126.70	0.920	0.00451	133.64	0.999
Zr/Ce-UiO-66-NH ₂	0.655	203.98	0.909	0.00399	216.16	0.999

Table 2 Langmuir and Freundlich model fitting parameters for U(VI) adsorption on Zr/Ce-UiO-66 and Zr/Ce-UiO-66-NH₂

Adsorbent	T (K)	Langmuir model			Freundlich model		
		q_e (mg g ⁻¹)	b (L mg ⁻¹)	R^2	K_f	$1/n$	R^2
Zr/Ce-UiO-66	298	293.87	0.271	0.990	60.33	0.472	0.864
	313	315.89	0.362	0.997	70.11	0.596	0.829
	328	566.14	0.194	0.991	84.90	0.411	0.872
Zr/Ce-UiO-66-NH ₂	298	376.80	0.093	0.994	57.97	0.528	0.849
	313	433.84	0.150	0.992	59.84	0.450	0.882
	328	611.33	0.221	0.996	68.84	0.497	0.925

Table 3 Different materials for U(VI) removal

Adsorbents experimental	Conditions (pH and T (K))	Capacity (mg g ⁻¹)	Ref.
UiO-66	5.5, 298	109.9	[19]
UiO-66-NH ₂	5.5, 298	114.9	[19]
P-Al ₂ O ₃ (MIL-53)	5.0, 298	316.87	[29]
MOF-76	3.0, 298	298	[30]
nZVI/UiO-66	6.0, 293	369	[39]
MMT@C	4.9, 333	105.98	[46]
Zr/Ce-UiO-66	6.0, 298	293.8	This work
Zr/Ce-UiO-66-NH ₂	6.0, 298	376.8	This work

Zr–O–Zr bond, and the other was the Zr and H₂BDC connection, specifically the Zr–O interconnection. Figures 7c and 8c show two Zr–O bonds at 183.20 eV and 185.50 eV. The peak at 185.50 eV corresponds to the Zr–O–Zr bond, whereas that at 183.15 eV represents the second type of Zr–O bond, which is consistent with prior research [45]. Figure 7c also shows that the Zr–O binding energy after uranium adsorption decreased from 183.15 eV to 182.53 eV. This phenomenon implies that Zr–O plays a significant role in uranium adsorption [45, 48]. A comparison of the O 1s spectra before and after uranium sorption (Figs. 7b and 8b) reveals shifts and peak changes. The intensities and areas of the peaks attributed to C–O and C=O decreased, whereas those attributed to Zr–O increased. These findings suggest that oxygen-containing functional groups facilitate U(VI) pre-enrichment throughout the reaction process. The surface complexes formed with U(VI) and various functional groups (specifically those containing C–O and C=O) significantly control the removal process. Meanwhile, the intensity of the N 1s peak (Figs. 4c and 3f) corresponding to the -NH₂ group

decreases significantly after U(VI) adsorption, suggesting that the amino groups play a significant role in uranium adsorption. The increased uranium-adsorption capacity of Zr/Ce-UiO-66-NH₂ also stems from this phenomenon.

After analyzing the above characterization and the kinetic and isothermal experimental results, we assessed the potential causes and mechanisms underlying the remarkable sorption performance of Zr/Ce-UiO-66-NH₂. Under the conditions of pH (pH=6) selected for the above experiments, the adsorption process is almost unaffected by the ionic strength. Functional groups such as N–H, C=O, C–O, Ce–O, and Zr–O were present on the surface of the material, where uranyl ions formed inner-sphere surface complexes by direct binding. In addition, at pH 6.0, UO₂²⁺ interacted with the negatively charged adsorbent via electrostatic attraction, resulting in prompt removal. The remarkable acid–base and chemical stability, exceptional adsorption capacity, and recyclability of Zr/Ce-UiO-66-NH₂, which was modified by a dual strategy of bimetalization and amination, suggest that the material has promising potential for wastewater treatment. A diagram of the adsorption mechanism is shown in Fig. 9.

4 Conclusion

In this study, a simple method was employed to synthesize the octahedral-structured nanomaterial Zr/Ce-UiO-66-NH₂. Dual strategies involving bimetalization and amination were adopted to extract uranium from aqueous solutions. Batch experiments demonstrated that, at pH 6.0, Zr/Ce-UiO-66-NH₂ had a uranium sorption ability of up to 376.8 mg · g⁻¹ and 611.33 mg g⁻¹ at 298 K and 328 K, respectively. These values were significantly better than the corresponding values for the bimetallic-modified Zr/Ce-UiO-66

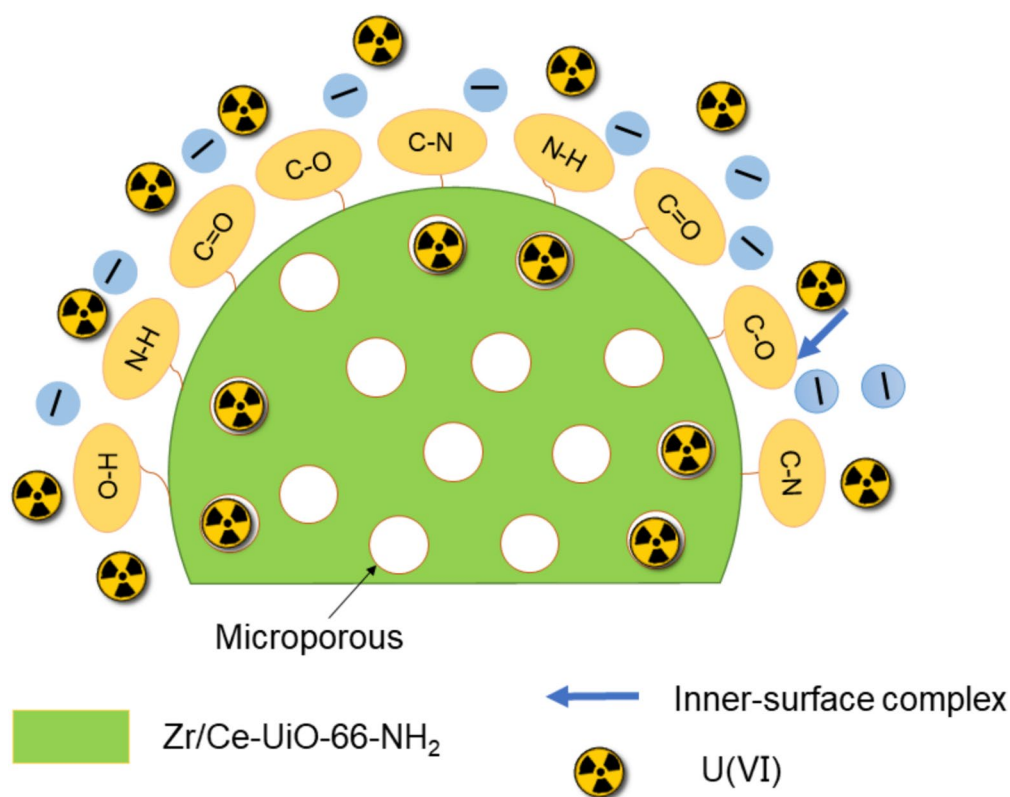


Fig. 9 Adsorption mechanism of U(VI) on Zr/Ce-UiO-66-NH₂. (Color figure online)

or the amine-functionalized UiO-66-NH₂. Kinetic and isotherm studies indicated that Zr/Ce-UiO-66-NH₂ undergoes spontaneous single-molecule chemisorption. Uranium ions are predominantly preserved in the material through chemical bonding to the active sites, forming internal surface complexes. Cycling experiments demonstrated good recovery performance and structural stability. The introduction of Ce exposes more active sites and increases the interaction of the substance with U(VI). Additionally, the incorporation of amino groups increases the number of binding sites. This facilitated the binding of uranium to Zr/Ce-UiO-66-NH₂. The possible adsorption mechanisms include internal surface complexation, chemisorption, and electrostatic interactions.

In brief, this study demonstrated the benefits of dual strategies for modifying Zr/Ce-UiO-66-NH₂ to remove hexavalent uranium, suggesting a promising application for treating uranium-containing wastewater.

Supplementary Information The online version contains supplementary material available at <https://doi.org/10.1007/s41365-024-01547-6>.

Author contributions All authors contributed to the study conception and design. Material preparation, data collection and analysis were performed by Wen-Hui Song, Chen Wang, Cheng-De Xie and Zhi-Xiong Zhang. The first draft of the manuscript was written by Wen-Hui Song and all authors commented on previous versions of the manuscript. All authors read and approved the final manuscript.

Data availability The data that support the findings of this study are openly available in Science Data Bank at <https://cstr.cn/31253.11.scienceadb.11415> and <https://www.doi.org/10.57760/sciencedb.11415>.

Declarations

Conflict of interest The authors declare no conflict of interest.

References

1. S. Zhang, L. Chen, Z. Qu et al., Confining Ti-oxo clusters in covalent organic framework micropores for photocatalytic reduction of the dominant uranium species in seawater. *Chem* **9**, 3172–3184 (2023). <https://doi.org/10.1016/j.chempr.2023.06.008>
2. N. Li, P. Gao, H. Chen et al., Amidoxime modified Fe₃O₄TiO₂ particles for antibacterial and efficient uranium extraction from seawater. *Chemosphere* **287**, 132137 (2022). <https://doi.org/10.1016/j.chemosphere.2021.132137>
3. G. Jiao, J. Ma, J. Zhang et al., Efficient extraction of uranium from seawater by reticular polyamidoxime-functionalized oriented holocellulose bundles. *Carbohydr. Polym.* **300**, 120244 (2023). <https://doi.org/10.1016/j.carbpol.2022.120244>
4. J. Dai, S. Li, J. Bi et al., The health risk-benefit feasibility of nuclear power development. *J. Clean. Prod.* **224**, 198–206 (2019). <https://doi.org/10.1016/j.jclepro.2019.03.206>
5. A. Biedrzycka, E. Skwarek, U. Margareta Hanna, Hydroxyapatite with magnetic core: synthesis methods, properties, adsorption and

- medical applications. *Adv. Colloid. Interfac.* **291**, 102401 (2021). <https://doi.org/10.1016/j.cis.2021.102401>
6. J. Ma, C. Wang, W. Xi et al., Removal of Radionuclides from aqueous solutions by manganese dioxide-based Nanomaterials and mechanism research: A review. *Acs. Est. Engg.* **1**, 685–705 (2021). <https://doi.org/10.1021/acsestengg.0c00268>
 7. Ü.H. Kaynar, Ü. Hiçsönmez, S. Çam Kaynar et al., Sorption of uranium(VI) from aqueous solutions by DEEA organo-volcanic: isotherms, kinetic, and thermodynamic studies. *Nucl. Sci. Tech.* **29**, 30 (2018). <https://doi.org/10.1007/s41365-018-0359-3>
 8. J. Zhang, J. Ma, G. Jiao et al., Methyl 4-hydroxybenzoate nanospheres anchored on poly(amidoxime)/polyvinyl alcohol hydrogel network with excellent antibacterial activity for efficient uranium extraction from seawater. *Desalination* **548**, 116243 (2023). <https://doi.org/10.1016/j.desal.2022.116243>
 9. J.H. Ye, T. Yu, Efficient and selective extraction of uranium from seawater based on a novel pulsed liquid chromatography radionuclide separation method. *Nucl. Sci. Tech.* **34**, 19 (2023). <https://doi.org/10.1007/s41365-023-01180-9>
 10. W.G. Cui, T.L. Hu, X.H. Bu, Metal-organic framework materials for the separation and purification of light hydrocarbons. *Adv. Mater.* **32**, 1806445 (2020). <https://doi.org/10.1002/adma.201806445>
 11. D.K. Singh, K.N. Hareendran, T. Sreenivas et al., Development of a phosphate precipitation method for the recovery of uranium from lean tenor alkaline leach liquor. *Hydrometallurgy* **171**, 228–235 (2017). <https://doi.org/10.1016/j.hydromet.2017.05.021>
 12. I. Mohammad, T. Hossain, Kinetics of water adsorption in UiO-66 MOF. *Ind. Eng. Chem. Res.* **58**, 10550–10558 (2019). <https://doi.org/10.1021/acs.iecr.9b00976>
 13. J.H. Cavka, S. Jakobsen, U. Olsbye et al., A new zirconium inorganic building brick forming metal organic frameworks with exceptional stability. *J. Am. Chem. Soc.* **130**, 13850–13851 (2008). <https://doi.org/10.1021/ja8057953>
 14. D.G. Piscopo, A. Polyzoidis, M. Schwarzer et al., Stability of UiO-66 under acidic treatment: Opportunities and limitations for post-synthetic modifications. *Micropor. Mesopor. Mat.* **208**, 30–35 (2015). <https://doi.org/10.1016/j.micromeso.2015.01.032>
 15. S. Tripathi, B. Sreenivasulu, A. Suresh et al., Assorted functionality-appended UiO-66-NH₂ for highly efficient uranium(VI) sorption at acidic/neutral/basic pH. *Rsc. Adv.* **10**, 14650–14661 (2020). <https://doi.org/10.1039/D0RA00410C>
 16. H. Liu, M. Cheng, Y. Liu et al., Modified UiO-66 as photocatalysts for boosting the carbon-neutral energy cycle and solving environmental remediation issues. *Coordin. Chem. Rev.* **458**, 214428 (2022). <https://doi.org/10.1016/j.ccr.2022.214428>
 17. J. Xiong, Y. Fan, F. Luo et al., Grafting functional groups in metal-organic frameworks for U(VI) sorption from aqueous solutions. *Dalton. T.* **49**, 12536–12545 (2020). <https://doi.org/10.1039/D0DT02088E>
 18. H. Zhang, A. Li, K. Li et al., Ultrafiltration separation of Am(VI)-polyoxometalate from lanthanides. *Nature* **616**, 482–487 (2023). <https://doi.org/10.1038/s41586-023-05840-z>
 19. Q. Chen, Q. He, M. Lv et al., Selective adsorption of cationic dyes by UiO-66-NH₂. *Appl. Surf. Sci.* **327**, 77–85 (2015). <https://doi.org/10.1016/j.apsusc.2014.11.103>
 20. B.C. Luo, L.Y. Yuan, Z.F. Chai et al., U(VI) capture from aqueous solution by highly porous and stable MOFs-UiO-66 and its amine derivative. *J. Radioanal. Nucl. Chem.* **307**, 269–276 (2016). <https://doi.org/10.1007/s10967-015-4108-3>
 21. L. Yang, X. Shan, Y. Zhao et al., Efficient phosphate capture of Fe₃O₄/UiO-66-NH₂/CeO₂ in wide pH spectrum. *Micropor. Mesopor. Mater.* **331**, 111653 (2022). <https://doi.org/10.1016/j.micromeso.2021.111653>
 22. Y. Fan, H. Zhang, M. Ren et al., Low-temperature catalytic degradation of chlorinated aromatic hydrocarbons over bimetallic Ce-Zr/UiO-66 catalysts. *Chem. Eng. J.* **414**, 128782 (2021). <https://doi.org/10.1016/j.cej.2021.128782>
 23. S.M. Shaikh, P.M. Usov, J. Zhu et al., Synthesis and defect characterization of phase-pure Zr-MOFs based on meso-tetracarboxy-phenylporphyrin. *Inorg. Chem.* **58**, 5145–5153 (2019). <https://doi.org/10.1021/acs.inorgchem.9b00200>
 24. L. Tan, P. Wang, R. Lu et al., Design and synthesis of hollow Ce/Zr-UiO-66 nanoreactors for synergistic and efficient catalysis. *J. Solid. State. Chem.* **312**, 123306 (2022). <https://doi.org/10.1016/j.jssc.2022.123306>
 25. M. Lammert, M.T. Wharmby, S. Smolders et al., Cerium-based metal organic frameworks with UiO-66 architecture: synthesis, properties and redox catalytic activity. *Chem. Commun.* **51**, 12578–12581 (2015). <https://doi.org/10.1039/C5CC02606G>
 26. F. Nouar, M.I. Breeze, B.C. Campo et al., Tuning the properties of the UiO-66 metal organic framework by Ce substitution. *Chem. Commun.* **51**, 14458–14461 (2015). <https://doi.org/10.1039/C5CC05072C>
 27. E. Geravand, F. Farzaneh, R. Gil-San-Millan et al., Mixed-metal cerium/zirconium MOFs with improved nerve agent detoxification properties. *Inorg. Chem.* **59**(22), 16160–16167 (2020). <https://doi.org/10.1021/acs.inorgchem.0c01434>
 28. J.M. Wang, S. Quan, R.Z. Zhang et al., Rapid adsorptive removal of cationic and anionic dyes from aqueous solution by a Ce (III)-doped Zr-based metal-organic framework. *Micropor. Mesopor. Mater.* **292**, 109764 (2020). <https://doi.org/10.1016/j.micromeso.2019.109764>
 29. S. Wang, Y. Bai, Z. Zhang et al., Simple construction of the α-MnO₂@ZIF-8 nanomaterial with highly enhanced U(VI) adsorption performance and assessed removal mechanism. *Prog. Nat. Sci-Mater. Int.* **33**, 508–517 (2023). <https://doi.org/10.1016/j.pnsc.2023.08.017>
 30. W. Yang, Z.Q. Bai, W.Q. Shi et al., MOF-76: from a luminescent probe to highly efficient U(VI) sorption material. *Chem. Commun.* **49**, 10415–10417 (2013). <https://doi.org/10.1039/C3CC44983A>
 31. B. Aguila, Q. Sun, J. Perman et al., Efficient mercury capture using functionalized porous organic polymer. *Adv. Mater.* **29**, 17006 (2017). <https://doi.org/10.1002/adma.201700665>
 32. Y.L. Wang, S. Zhang, Y.F. Zhao et al., UiO-66-based metal organic frameworks for the photodegradation of acetaminophen under simulated solar irradiation. *J. Environ. Chem. Eng.* **9**, 106087 (2021). <https://doi.org/10.1016/j.jece.2021.106087>
 33. X.Y. Min, X. Wu, P.H. Shao et al., Ultra-high capacity of lanthanum-doped UiO-66 for phosphate capture: unusual doping of lanthanum by the reduction of coordination number. *Chem. Eng. J.* **358**, 321–330 (2019). <https://doi.org/10.1016/j.cej.2018.10.043>
 34. Z. Man, Y. Meng, X.C. Lin et al., Assembling UiO-66@TiO₂ nanocomposites for efficient photocatalytic degradation of dimethyl sulfide. *Chem. Eng. J.* **431**, 133952 (2022). <https://doi.org/10.1016/j.cej.2021.133952>
 35. Y. Li, Q. Yin, Y.S. Zeng et al., Hollow spherical biomass derived-carbon dotted with SnS₂/gC₃N₄ Z-scheme heterojunction for efficient CO₂ photoreduction into CO. *Chem. Eng. J.* **438**, 135652 (2022). <https://doi.org/10.1016/j.cej.2022.135652>
 36. F. Xu, Q. Zhang, R. An, L. Li, L. Zhou, Facile fabrication of flower-like NH₂-UiO-66/BiOCl Z-scheme heterojunctions with a significantly improved photocatalytic performance for tetracycline removal under solar irradiation. *J. Alloy. Compd.* **899**, 163324 (2022). <https://doi.org/10.1016/j.jallcom.2021.163324>
 37. L. Ding, F.H. Bai, B. Borjigin et al., Embedding Cs₂AgBiBr₆ QDs into Ce-UiO-66-H to in situ construct a novel bifunctional material for capturing and photocatalytic reduction of CO₂. *Chem. Eng. J.* **446**, 137102 (2022). <https://doi.org/10.1016/j.cej.2022.137102>

38. Y.X. Mei, N.C. Yuan, Y.T. Xie et al., Facile fabrication of the direct Z-scheme heterojunction of $\text{NH}_2\text{-UiO-66}$ and CeCO_3OH for photocatalytic reduction of CO_2 to CO and CH_4 . *Appl. Surf. Sci.* **597**, 153725 (2022). <https://doi.org/10.1016/j.apsusc.2022.153725>
39. Y.J. Zhou, Z.M. Mao, W. Wang et al., In-situ fabrication of graphene oxide hybrid Ni-based metal-organic framework (Ni-MOFs@GO) with ultrahigh capacitance as electrochemical pseudocapacitor materials. *ACS Appl. Mater. Inter.* **8**(42), 28904–28916 (2016). <https://doi.org/10.1021/acsami.6b10640>
40. F. Yang, S. Xie, G. Wang et al., Investigation of a modified metal-organic framework UiO-66 with nanoscale zero-valent iron for removal of uranium (VI) from aqueous solution. *Environ. Sci. Pollut. R.* **27**, 20246–20258 (2020). <https://doi.org/10.1007/s11356-020-08381-4>
41. L.M. Yin, D.B. Wang, X.P. Li et al., One-pot synthesis of oxygen-vacancy-rich Cu-doped UiO-66 for collaborative adsorption and photocatalytic degradation of ciprofloxacin. *Sci. Total. Environ.* **815**, 151962 (2022). <https://doi.org/10.1016/j.scitotenv.2021.151962>
42. X. Wang, Y. Wang, G. Chai et al., Poly (triphenylamine)-decorated UiO-66- NH_2 mesoporous architectures with enhanced photocatalytic activity for CO_2 reduction and H_2 evolution. *J. CO_2 Util.* **51**, 101654 (2021) <https://doi.org/10.1016/j.jcou.2021.101654>
43. A. Valverde-Gonzalez, M. Pintado-Sierra, A. Rasero-Almansa et al., Amino-functionalized zirconium and cerium MOFs: catalysts for visible light induced aerobic oxidation of benzylic alcohols and microwaves assisted NAlkylation of amines. *Appl. Catal. A-Gen.* **623**, 11828 (2021). <https://doi.org/10.1016/j.apcata.2021.118287>
44. N. Gumber, R.V. Pai, K. Sanyal et al., Synthesis and uranium adsorption studies of UiO-66 (Ce) based metal organic frameworks from aqueous solutions. *Micropor. Mesopor. Mat.* **341**, 112108b (2022). <https://doi.org/10.1016/j.micromeso.2022.112108>
45. W. Yao, X. Wang, Y. Liang et al., Synthesis of novel flower-like layered double oxides/carbon dots nanocomposites for U(VI) and $^{241}\text{Am(III)}$ efficient removal: batch and EXAFS studies. *Chem. Eng. J.* **332**, 775–786 (2018). <https://doi.org/10.1016/j.cej.2017.09.011>
46. Y.W. Cai, M. Fang, B.W. Hu et al., Efficient extraction of U(VI) ions from solutions. *Nucl. Sci. Tech.* **34**, 2 (2023). <https://doi.org/10.1007/s41365-022-01154-3>
47. M. Zhang, M. Yuan, X. Zhao et al., Radiation-induced one-pot synthesis of grafted covalent organic frameworks. *Sci. China Chem.* **66**, 1781–1787 (2023). <https://doi.org/10.1007/s11426-022-1532-8>
48. S. Song, S. Huang, R. Zhang et al., Simultaneous removal of U(VI) and humic acid on defective TiO_{2-x} investigated by batch and spectroscopy techniques. *Chem. Eng. J.* **325**, 576–587 (2017). <https://doi.org/10.1016/j.cej.2017.05.125>
49. Y. Zhao, C. Guo, H. Fang et al., Competitive adsorption of Sr(II) and U(VI) on graphene oxide investigated by batch and modeling techniques. *J. Mol. Liq.* **222**, 263–267 (2016). <https://doi.org/10.1016/j.molliq.2016.07.032>
50. P. Li, Y. Wang, J. Wang et al., Carboxyl groups on g- C_3N_4 for boosting the photocatalytic U(VI) reduction in the presence of carbonates. *Chem. Eng. J.* **414**, 128810 (2021). <https://doi.org/10.1016/j.cej.2021.128810>

Springer Nature or its licensor (e.g. a society or other partner) holds exclusive rights to this article under a publishing agreement with the author(s) or other rightsholder(s); author self-archiving of the accepted manuscript version of this article is solely governed by the terms of such publishing agreement and applicable law.